Time and Frequency Blanking for Radio Frequency Interference Mitigation in Microwave Radiometry

B. Güner, J. T. Johnson, and N. Niamsuwan

***Abstract*— Radio frequency interference (RFI) is a major limiting factor in passive remote sensing and radio astronomy. A digitally-based radiometer system has been developed at The Ohio State University ElectroScience Laboratory (OSU/ESL) to improve RFI mitigation through the use of high temporal and spectral resolution. The system includes a pulse-blanking algorithm that is capable of removing pulsed time-domain sources in real time. Cross-frequency mitigation is also possible in post-processing through use of the system's high spectral resolution.**

Several experiments have been conducted at L- and C- bands in recent years. Datasets from two particular campaigns are analyzed in this paper: ground-based observations at L-band in Canton, Michigan that emphasize pulse blanking and an airborne campaign at C-band over Texas and the Gulf of Mexico that emphasizes cross-frequency mitigation. Results and analyses are presented to quantify the RFI mitigation performance achieved.

I. Introduction

RECENT measurements with space-borne Earth observing radiometers have shown significant corruption of C-band brightness temperatures due to radio frequency interference (RFI) [1]-[2]. Since there is no portion of the C-band spectrum for which transmissions are prohibited, microwave radiometers operating in this band for sensing soil moisture, sea surface temperature, or other geophysical parameters require a means for mitigating RFI. At L-band, although the frequency range 1400-1427 MHz is protected, RFI sources operating very close to these frequencies may still degrade radiometric measurements. Also, operation in a bandwidth larger than the protected 27 MHz would be preferable if possible to increase the sensitivity of the radiometer to several geophysical parameters. While the detection and mitigation of RFI is an important issue for radiometry in general, C- and L-bands are of particular interest at present due to their use in current and future systems.

Many current RFI mitigation techniques rely on the facts that RFI always increases the observed brightness beyond that due to the thermal noise alone and that anthropogenic emissions are almost always localized in time or frequency. Therefore, if sufficient temporal or spectral resolution is obtained, it is possible to distinguish unnatural increases in brightness caused by time or frequency localized RFI sources [3]-[5]. Other RFI detection strategies have also been proposed based on examination of the statistics of the received fields [6], but such approaches are not considered here. The use of digitally based receiver hardware as compared to traditional analog systems is advantageous for RFI detection and mitigation due to a digital receiver's inherently high temporal sampling rate and ability to obtain a large number of frequency channels with little additional complexity. With these goals in mind, digitally based radiometers have been under investigation at the Ohio State University ElectroScience Laboratory since 2002 [7]. The systems developed have performed successfully in several airborne and ground-based demonstrations at L- and C-bands [8]-[12]. Henceforth, the version of the digital radiometer utilized for L-band observations is called the L-band Interference Suppressing Radiometer (LISR), while the version used at C-band is called the C-band Interference Suppressing Radiometer (CISR). Both systems include a real time pulse-blanking algorithm (called asynchronous pulse blanking (APB) in what follows) implemented in digital hardware, and both achieve high frequency resolution through an FFT operation again performed in digital hardware. The latter allows mitigation of frequency localized sources through post-processing analyses.

In this paper, the mitigation performance achieved by time and frequency domain blanking is assessed. A discussion of time domain blanking follows in Section 2 through use of data obtained from an L-band ground-based campaign in Canton, Michigan [8]. This campaign was performed in close proximity to a pulsed radar system operating at a frequency close to the radiometer's passband, and hence is useful for showing the effectiveness of the APB algorithm. Results from an airborne campaign at C-band over Texas and the Gulf of Mexico [11] are described in Section 3, and are used to examine the effectiveness of frequency domain blanking in a complex RFI environment. Final conclusions and discussions are provided in Section 4.

II. L-band Observations of an ARSR System in Canton, MI

Data from a ground-based campaign involving L-band observations in close proximity to an air-route surveillance radar (ARSR) located in Canton, MI on June 16^{th} and June 17^{th}, 2005 are used to demonstrate RFI mitigation in the time domain. This campaign (which will be denoted as the Canton campaign) was conducted by researchers from the University of Michigan [6], NASA Goddard Space Flight Center, and The Ohio State University, and included advanced RFI mitigating radiometer "backends" from each of these organizations. A truck-mounted L-band radiometer front-end supplied by the University of Michigan was placed within approximately 200 m. of the ARSR antenna, ensuring that strong out-of-band interference would be experienced in the observations. The experiment was designed to demonstrate that the backends developed could successfully remove interference in both

The Ohio State University, Department of Electrical and Computer Engineering and ElectroScience Laboratory, 1320 Kinnear Road, Columbus, OH 43210, USA. Email: johnson.1374@osu.edu

extremely strong and slight interference environments. The latter case was obtained through choice of the observation direction of the radiometer antenna, as well as the fact that the radar center frequency (reported as 1315 MHz by the station's literature) was far out-of-band of the radiometer observations. Other properties of the radar reported by the station are a peak radiated power of 4 MW, an antenna gain of 35 dB, an antenna tilt angle of 2.6 degrees, a typical PRF of 360 Hz, and a pulse width of 2 μsec.

A. Instrumentation

The L-band radiometer front-end contained dual receivers so that simultaneous observations of horizontal and vertical polarization were provided. The system utilized a large L-band horn antenna with a half power beamwidth of $20°$, and included internal calibration standards so that the antenna temperature could be directly computed from measured data. Results will be reported as calibrated antenna temperatures, not the brightness temperature of the observed scene, as external calibration standards were not available in the campaign. Use of the antenna temperature rather than the scene brightness temperature is not expected to have any significant impact on an assessment of RFI mitigation performance.

RF filters within the radiometer front end set the RF 3-dB bandwidth as 1403.5 MHz to 1423.5 MHz. The RF signal is downconverted with an LO at either 1386.5 or 1440.5 MHz such that an IF frequency bandwidth of 17-37 MHz is obtained; image rejection in the downconversion process is provided by the RF front end filters. IF outputs for both polarizations were then power divided and supplied to the three backend systems.

A block diagram of LISR as configured for this experiment is provided in Figure 1. LISR samples both the incoming H and V pol 17-37 MHz IF's at 100 MSPS, using 10-bit A/D converters for this purpose. The subsequent LISR operations described in Figure 1 take place in a single field-programmable gate array (FPGA). First, the incoming IF's are digitally filtered and then combined into a single complex datastream at 100 MSPS. The digital filter used has a bandwidth wider than that set by the RF filters, and therefore has little impact on the measured data. However, its use allows removal of the image spectrum for each of the input polarizations so that the combination into a single 100 MSPS complex datastream is possible.

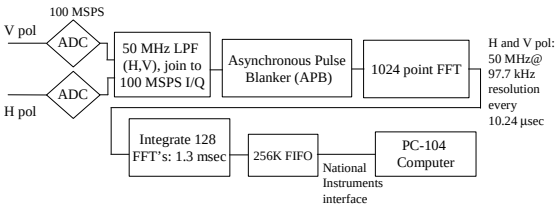

Fig. 1. LISR block diagram

Following this output is a set of processors that can be controlled by the operator in real time through an ethernet interface between the system computer and the FPGA. In the results presented here, LISR was operated in three distinct modes, labeled "Integration, APB off", "Integration, APB on", and "Capture" in what follows.

In "Capture" mode, the 100 MSPS complex datastream is directly passed to the control and recording computer without further processing. The high temporal resolution and coherent data acquired allow detailed studies of the properties of the observed interference. Results from this mode are not presented here, but are available in [8].

The other LISR modes utilize data that has passed through the asynchronous pulse blanking stage. The APB is designed to detect and blank radar pulses in real time, so that their effects can be removed without further processing while maintaining accurate calibration of the noise-free data [13]. The basic operation principle of the APB is illustrated in Figure 2. To detect pulsed interferers, the APB maintains a running estimate of the mean and variance of the incoming power in the time domain (through use of an exponential averaging operation as described in [13].) Whenever a sample power greater than a threshold number of standard deviations from the mean is detected, the APB blanks (sets to zero) a block of samples of length NBLANK beginning from a predetermined period before the triggering sample (shown as NWAIT in the figure), through and hopefully including any multi-path components associated with the detected pulses. APB operating parameters are adjustable and can be set by the user. In the experiments described here, the APB threshold was set to 9 standard deviations from the mean power level, and a blanking window of 40 μsec was used (note 40 μsec corresponds to 6 km of radar range.) This window began 10.24 μsec prior to the detected sample. The APB provides information on the amount of blanking to further processor stages so that blanking effects on calibration can be corrected in real time.

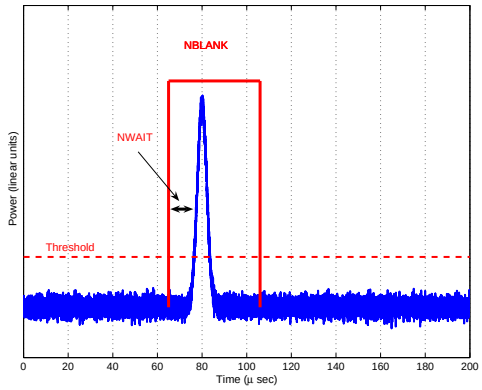

Fig. 2. Basic operation procedure of APB

The expected false-alarm rate (i.e. fraction of samples blanked when the input fields are RFI-free Gaussian noise) of the APB processor can ideally be determined analytically as a function of the detection threshold and other APB parameters. Given the Nyquist sampled complex datastream input to the APB, individual sample powers are exponential random

variables, and the probability of exceeding the mean power by a specified number of standard deviations can be determined easily. However, the APB processor also controls the number of blanking "windows" that can be created within a specified time period, as described in [13], making analytical evaluation of the false alarm rate difficult. Monte Carlo simulations of the APB processor were instead utilized to determine that 1.6% of samples were blanked under RFI-free conditions for the APB parameters of the Canton campaign; this result was found consistent with the percent blanking observed for the internal calibration standards in the experiment. Again the effect of blanking is compensated for when computing averages, as described in [13], and laboratory results confirm that average RFI-free brightnesses are unaffected by the blanking process.

Following the APB is a length-1K complex FFT utilizing a triangular window to reduce truncation effects. This FFT operation provides an output every 10.24 μsec, with two sets of 512 bins obtained in two corresponding 50 MHz bandwidths; the first set is for horizontal and the second set for vertical polarization. The resulting spectral resolution is approximately 97 kHz, much finer than the bandwidth of many expected RFI sources. FFT outputs are then passed through detection and integration operations, with the final datastream comprised of 1024 frequency bins obtained every 1.3 msec.

The distinction between "Integration, APB on" and "Integration, APB off" modes involves whether the APB blanking is turned on or off in the data input to the FFT operation. Comparing brightnesses obtained in these modes allows the effectiveness of the APB real-time pulse removal algorithm to be examined. Results following integration are stored in a 32 bit, 256K FIFO and then passed through a National Instruments interface to the system control computer. The basic antenna observations consisted of 205 spectra (262.4 msec integration time) acquired and transferred to the system computer before the front end switched to internal load observations.

B. Time Domain Blanking Results

Strong and weak RFI cases were produced in the campaign by changing the observation direction of the antenna; the radar was located at an azimuth angle of approximately 160° with respect to the default position of the antenna. Therefore, data obtained at azimuthal observation angles of 0° and 160° will be compared to show the effectiveness of the APB algorithm in the "weak" and "strong" cases, respectively. In both cases, the elevation angle of the antenna was 1°.

Figures 3 and 4 plot calibrated antenna temperatures in vertical and horizontal polarizations, respectively, for both "Integration, APB on" and "Integration, APB off" modes when the azimuth angle was 0°. The scene included within the antenna pattern consisted of a nearby forest as well as the sky. Note that "Integration, APB on" and "Integration, APB off" modes were not observed simultaneously: the results shown are an average of data on June 17^{th} from 14:51:43-14:56:15 UTC for "Integration, APB off" mode (around 110 seconds of antenna observation time) and 14:56:43-14:58:19 UTC time for "Integration, APB on" mode (around 39 seconds of antenna observation time). Due to the short time delay between the observations we can assume that the natural radiation observed was relatively similar in both cases; note there is a slight trend of antenna temperatures versus frequency that is consistent with expected loss properties of the antenna as a function of frequency. The horizontal axis of these figures is the RF frequency, mapped from the LISR IF frequencies of 0 to 50 MHz for the LO Frequency of 1440.5 MHz, and truncated to the range 1399 to 1427 MHz.

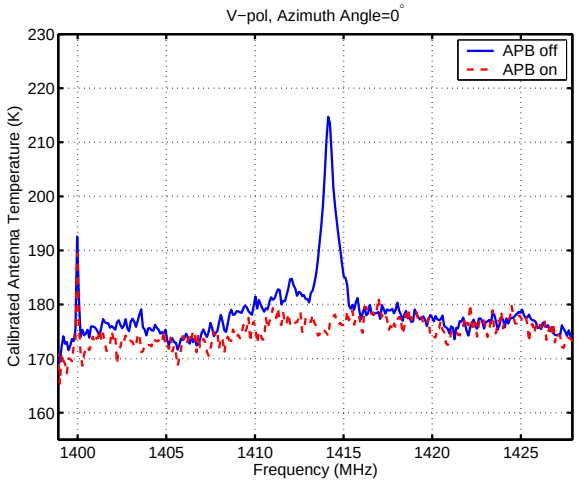

Fig. 3. Average calibrated antenna temperature versus frequency, V pol, azimuth angle=0°

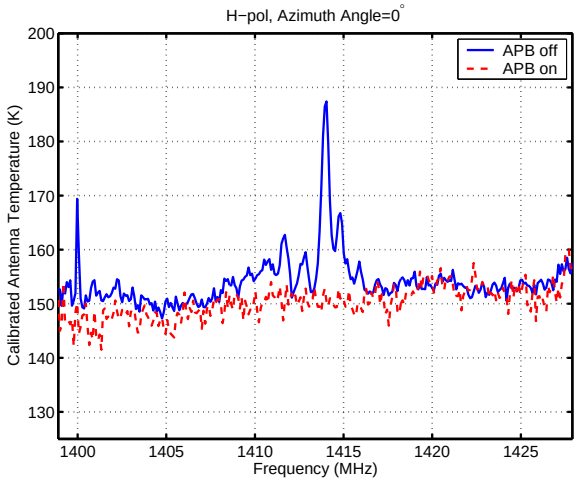

Fig. 4. Average calibrated antenna temperature versus frequency, H pol, azimuth angle=0°

Narrowband emissions near 1400 MHz can be observed for both polarizations; this source is apparently more continuous in nature so that the APB status has only limited impact. The exact origin of this source is not known, although similar emissions have been observed in other campaigns at a variety of locations, suggesting that emissions from some variety of consumer electronics or computer devices may be responsible.

Another strong RFI source in the range 1410-1415 MHz is observed for both polarizations that is dramatically reduced in the "Integration, APB on" mode. If 1315 MHz ARSR emissions received by the radiometer antenna due to scattering

from the forest scene are insufficiently attenuated by the radiometer frontend filters, the resulting IF frequency is 125.5 MHz or 71.5 MHz for LO frequencies 1440.5 MHz and 1386.5 MHz, respectively. When sampled at 100 MSPS, these frequencies are mapped to RF frequency 1415 MHz. Thus, the 1410-1415 RFI source originates from the radar, and is successfully mitigated by the APB. The APB processor reported approximately 3% blanking of samples in this case, reasonably consistent with a combination of the 1.6% reported for the internal calibration loads and the 1.4% that results from blanking a 40 μsec window at the known radar PRF.

Figure 5 plots V-pol and H-pol total channel antenna temperatures in the band 1399-1428 MHz versus time for both APB on and APB off modes. Results show the APB on data to have a mean antenna temperature around 3 K less than that of the APB off data, due to the removal of RFI contributions in the APB on case. The APB on data also exhibits much smaller variations among samples compared to the APB off results. These results show that the APB algorithm is extremely effective in this RFI environment, even with apparently "weak" pulses (RFI contributions comparable to possible geophysical variations and to the antenna temperature's standard deviation) when integrated over time and the radiometer bandwidth.

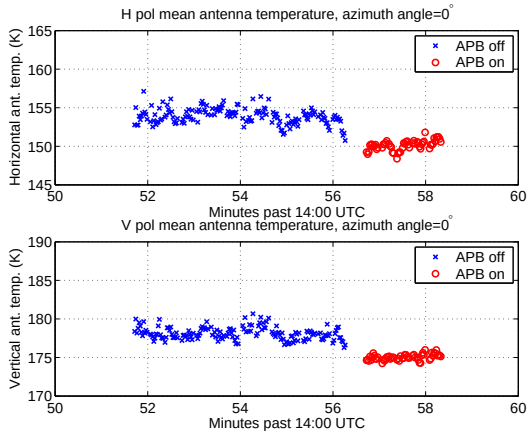

Fig. 5. Calibrated V-pol LISR data in the band 1399-1428 MHz versus time, for both APB off and APB on modes when azimuth angle is 0°. The upper plot shows horizontal polarization, and the lower plot shows vertical polarization

Figures 6 and 7 provide the same results when the antenna was looking directly at the radar (i.e azimuth angle is 160°). Calibrated antenna temperatures shown are an average of observations on June 17^{th} between 15:51:55-15:53:10 for "Integration, APB off" mode and 15:53:40-15:53:58 for "Integration, APB on" mode. Again, the horizontal axis shows the RF frequency mapped from the IF frequency, but the LO frequency was 1386.5 MHz in this case. The APB processor reported a similar fraction of samples blanked as in the 0 degrees azimuth angle case.

The level of the antenna temperature in "Integration, APB off" mode is higher than the APB on mode for almost all frequencies, which suggests that pulse amplitudes are sufficiently high to cause some degree of saturation within the digital receiver processing. Continuous RFI sources at 1400

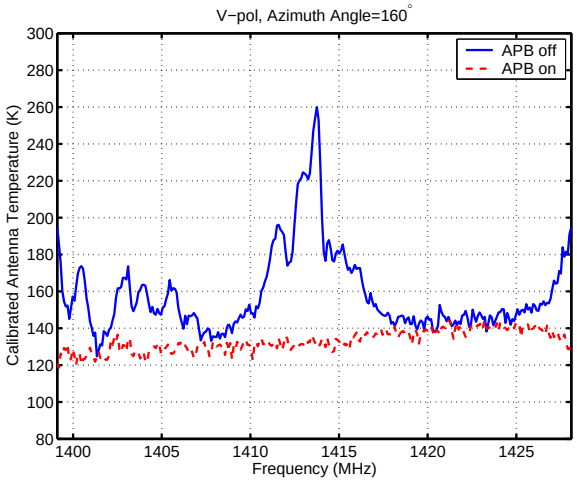

Fig. 6. Average calibrated antenna temperature versus frequency, V pol, azimuth angle=160°

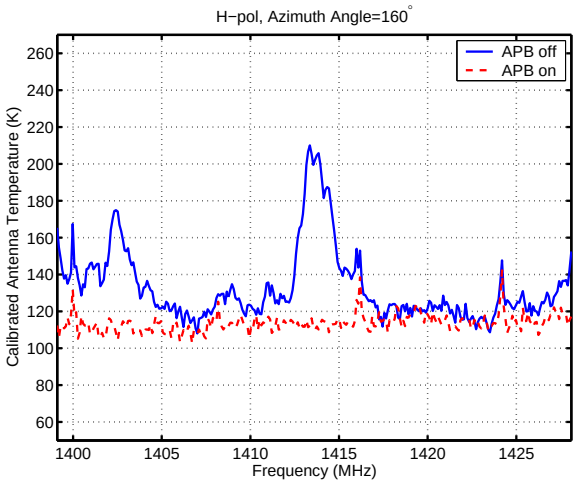

Fig. 7. Average calibrated antenna temperature versus frequency, H pol, azimuth angle=160°

MHz, 1417 MHz, and 1424 MHz apparently associated to some degree with the radar emissions can be observed for horizontal polarization which are not strongly affected by the APB.

The maximum antenna temperature in "Integration, APB off" mode occurs around 1414 MHz for both polarizations, and again is significantly reduced along with the apparent saturation effects by the APB algorithm. Figure 8 illustrates total channel antenna temperatures over an extended time period for this case, showing much larger differences (up to 20 K) between the APB on and off cases than in Figure 5. While RFI in this case would be more easily detectable due to the high levels observed, the APB algorithm removes these effects in real time without requiring further processing of data, and allows continued observations even in the presence of strong RFI. Note remaining narrowband, non-pulsed emissions can be removed through use of the cross-frequency algorithms discussed in the next Section; such results are shown in [8].

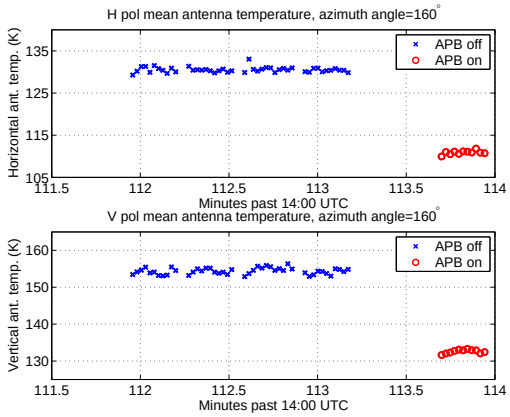

Fig. 8. Same as Figure 5, but when azimuth angle is 160°.

III. Airborne C-band RFI measurements and Cross Frequency Blanking

Frequency domain blanking of RFI is discussed for data obtained from observations at C-band made from NASA's WB-57 high-altitude aircraft using the PSR/CXI radiometer system of the University of Colorado and the CISR digital backend. These observations were performed during a test flight on Aug. 25^{th}, 2005 beginning at Ellington Field, Houston, TX and including overflights of Dallas and San Antonio as well as a flight segment over the Gulf of Mexico. Figure 9 illustrates the geographical region observed and includes UTC flight times along the path; note major cities including Houston, Dallas-Fort Worth, and San Antonio are marked with circles.

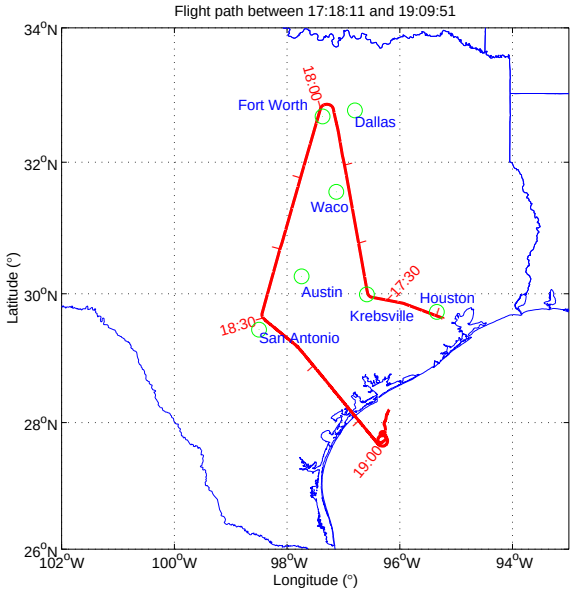

Fig. 9. Flight path, including nearby Texas cities (circles) for the WB-57 campaign

A. Instrumentation

The PSR/CXI system used for the antenna and front end has been deployed in several previous airborne remote sensing campaigns [3], and provides well calibrated scene brightness temperature measurements along with a variety of possible scanning patterns during flight operations. The data presented here are from conically scanned operations (i.e the antenna is rotated in azimuth at a fixed speed) at a fixed incidence angle of 55° from nadir. The antenna 3dB beamwidth is approximately 10°. When in conical scan mode, the PSR/CXI antenna rotation period was typically 40 seconds.

The PSR/CXI instrument includes four C-band subchannels, with respective frequency ranges of 5.8-6.2,6.3-6.7, 6.75-7.1, and 7.15-7.5 GHz. The system includes a downconverter module with an image reject mixer to produce 22 tuned 100 MHz channels between 5.5 GHz and 7.7 GHz that are observed by the CISR backend. The local oscillator was swept continuously throughout the flight, with each channel and internal calibration loads being observed for approximately 37 msec; a complete sweep of channels required approximately 814 msec. A portion of the tuned signal for V pol was coupled to CISR; CISR did not measure H pol in this experiment. The CISR digital receiver backend measures the incoming signal using two 200 MSPS A/D converters to obtain a 100 MHz sampled signal. The remaining CISR operations starting with the APB are identical to those of LISR. The CISR system used is similar in general to that described in more detail in [9], with slight modifications to improve survivability in the high altitude environment. "Integration, APB off" and "Capture" modes were utilized in this experiment. In the "Integration, APB off" data to be examined here, a base temporal resolution of 1.3 msec was used, with 12 1024 point spectra obtained in 15.75 msec for antenna observations in each tuned channel.

B. Frequency-Domain Mitigation

The WB-57 campaign represents a very dynamic RFI environment, with differing RFI sources observed as the tuned channel is swept through C-band and as the aircraft location changes. As seen in Figure 9, the flight path included major urban centers, rural areas, and the Gulf of Mexico, all of which involve differing RFI properties. Because pulsed sources are not common at C-band, the cross-frequency mitigation method is emphasized here through post-processing of measured data. Since naturally emitted thermal noise is expected to vary slowly with frequency, and since CISR has a very high spectral resolution, cross frequency mitigation should be very effective against RFI that is localized in frequency.

A cross-frequency mitigation technique was applied to calibrated data. For a particular observation, we have brightness temperatures in 1024 frequency bins of approximately 97 kHz each as a result of the FFT operation. The algorithm operates on a single set of 1024 frequency bins averaged to 15.75 msec time resolution, as follows:

1) First, an acceptable brightness temperature range is set depending on the scene observed. Frequency bins with brightnesses outside the acceptable range are marked as corrupted. For land observations, the acceptable range was set as 200 K to 400 K.
2) The standard deviation and mean (both over frequency) of brightnesses are found for the lowest 85% (in terms

of brightness) of the remaining frequency bins (to avoid bias of the mean and standard deviation by RFI). Another threshold test is then applied: frequency bins that are more than 4 standard deviations from the mean over frequency are marked as corrupted. Neighboring frequency bins within 4 frequency bins of the corrupted bins are marked as well.

3) Brightness temperatures of corrupted bins are replaced with the mean of the remaining frequency bins.

This algorithm is relatively simple compared to other cross-frequency algorithms that have been developed for a smaller number of channels [3], [9]. However it will be shown to be successful in removing much of the observed RFI in what follows. Simplicity in the algorithm is desirable in order to make future implementation in digital hardware feasible. Because a future hardware implementation would likely utilize uncalibrated data, rather than calibrated data as in the current algorithm, continued work will be required to develop an approach that incorporates power variations with frequency caused by the system passband response.

While it is again possible ideally to predict the false-alarm rate of this algorithm, the consideration of neighboring frequency bins in the cross-frequency blanking process complicates the analysis. A Monte Carlo analysis however showed the false alarm rate for the specified algorithm to be $\approx 2\%$. These false alarms do not impact obtained mean brightnesses due to the replacement of detected bin brightnesses with the average of the remaining brightnesses.

As an example of the algorithm's performance, Figure 10 plots a comparison of unmitigated and mitigated brightness temperatures versus UTC time for CISR channels 8, 12, 16, and 20 during a one-hour portion of the flight (all over land). These total channel brightnesses were calculated by taking the average of calibrated brightnesses in the 1024 CISR frequency bins corresponding to a 100 MHz bandwidth. Channel 8 represents observations from 6.2 to 6.3 GHz, channel 12 is 6.6 GHz to 6.7 GHz, channel 16 is 7 to 7.1 GHz, and channel 20 is 7.4 to 7.5 GHz. The brightness temperature points shown are averaged over observations in the specified channel during a 40 sec. time period; this is equal to one period of the antenna's conical scan. Time periods with no points in the figures correspond to times when the antenna was not in conical scanning mode or when it observed external hot or cold load targets for calibration purposes.

All four of these channels (as well as the CISR channels not plotted) show significant RFI corruption, with brightnesses averaged over 40 seconds exceeding 400 K in some cases, and the level of RFI corruption shows a significant variation over time. In measurements around 18:00 UTC when the aircraft was over the Dallas-Fort Worth area, all channels show large brightness temperatures. The higher frequency channels show less RFI corruption compared to the lower frequency channels, which is in accordance with the expected higher source densities at lower frequencies. However, all channels show at least 50 K of RFI contributions at some instant during this interval. Results following application of the cross-frequency mitigation procedure show a greatly reduced impact of RFI. One interesting observation in general is that, although all 22 CISR channels were mitigated separately, mitigated brightnesses are very similar in each channel as should be expected for thermal noise measurements. Variations of the mitigated temperatures with time also are consistent with expectations for observations over geophysical landscapes.

A more detailed time history of channel 16 (without any averaging of the observed data over time) is presented in the lower half of Figure 11 for an approximately 90 sec. portion of the flight over the Dallas-Fort Worth area. As this is an urban scene, it is not surprising that a high degree of RFI activity with an apparent period of ≈40 sec. (the antenna rotation time) can be observed. The mitigation algorithm significantly reduces this RFI. The results also show that portions of the time history without obvious RFI have similar brightnesses before and after the mitigation algorithm. However, RFI mitigations as large as 215 K are observed in some cases. "Spectrogram" images of brightnesses for the original and mitigated data for the same time period are also shown in Figure 11 (two upper plots). The horizontal axis is UTC time and the vertical axis is frequency in MHz for these images. The source of the periodic brightness increases in the time domain plot can be seen clearly here, including apparent sources near 7010, 7040, 7060, 7070, and 7090 MHz. The mitigated data image shows that the algorithm developed removes these contributions.

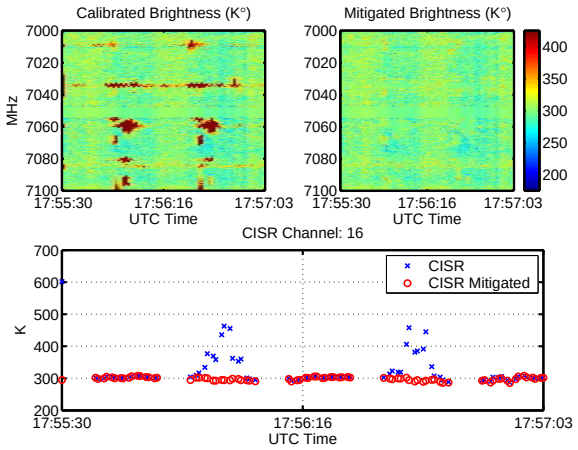

Fig. 11. Spectrogram images and time history of brightness temperatures for original and mitigated data over an urban landscape, CISR channel 16

An example of observations in CISR channel 8 over the Gulf of Mexico is provided in Figure 12. The plot of total channel brightness versus time (lower plot) is not completely free of RFI even in these at-sea observations. For this case, sources near 6204 MHz and 6282 MHz are successfully mitigated, as shown in the spectrogram images in the upper portion of the figure. Although the contribution of these RFI sources to the total channel brightness is smaller than in the case of observations in the Dallas-Fort Worth area, brightness increases near 45 K can still be observed.

To demonstrate cross frequency mitigation performance for weak RFI environments, a 45 sec. observation over a rural area between Fort Worth and San Antonio is used. A comparison of original and mitigated data for CISR channel 17 (7.1 GHz-7.2 GHz) is provided in Figure 13, again with

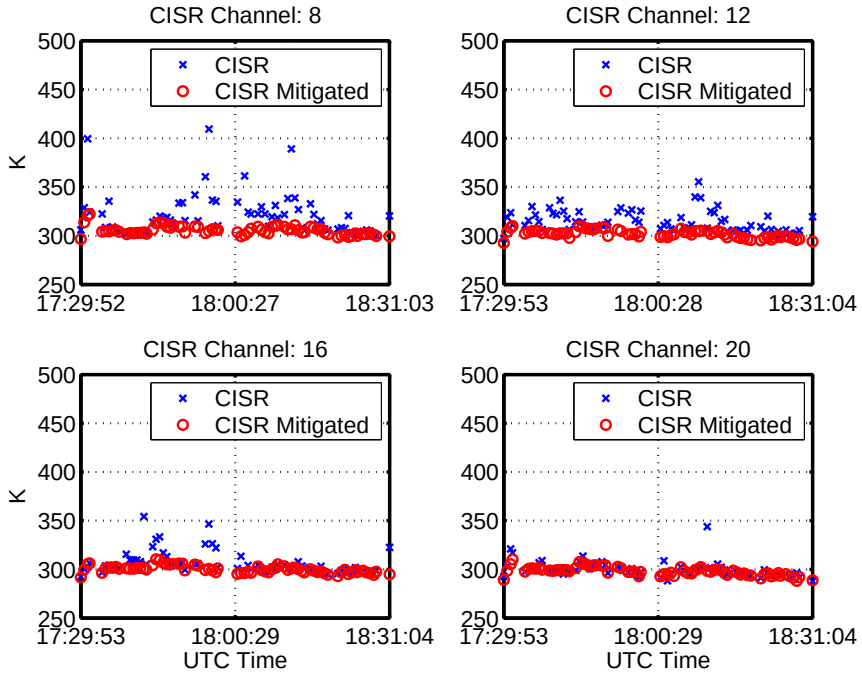

Fig. 10. Comparison of calibrated brightness temperatures vs. time between original and mitigated data for CISR channels 8,12,16 and 20

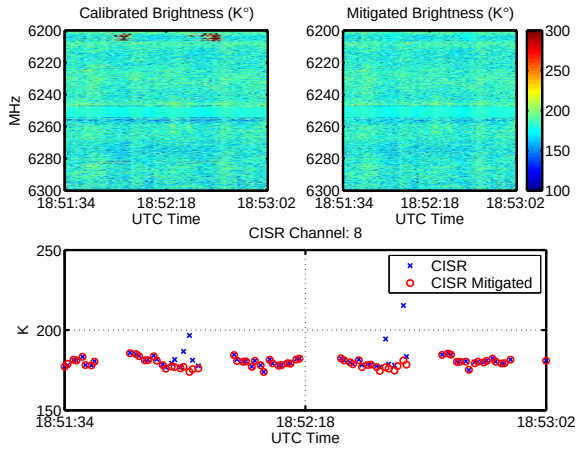

Fig. 12. Spectrogram images and time history of brightness temperatures for original and mitigated data over the Gulf of Mexico, CISR channel 8

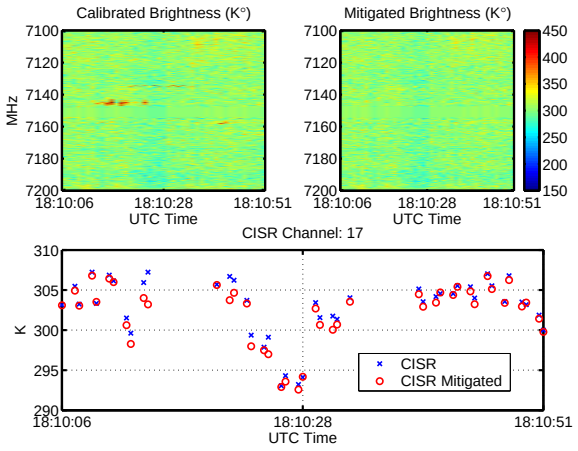

Fig. 13. Spectrogram images and time history of brightness temperatures for original and mitigated data over a rural landscape, CISR channel 17

the time history of total channel brightnesses in the lower plot and brightness spectrograms in the upper plots. Narrowband interferers around 7107, 7135, 7145 and 7157 MHz are observed in original brightness image, with 7145 MHz having the largest amplitude; the mitigated image indicates removal of these sources. The time history plot demonstrates that the contributions of these detected RFI sources to the brightness of the 100 MHz channel are in the range 1-3 K, and comparable to the estimated radiometer brightness standard deviation of 1.5 K. Such low level RFI is very difficult for a traditional radiometer to detect because it is within the range of the instrument sensitivity as well the range of expected geophysical brightnesses; the high spectral resolution of CISR however allows these narrowband but large amplitude sources (i.e. amplitudes more than four standard deviations from the mean brightness over frequency) to be readily detected and removed.

IV. Conclusions

Results from L- and C-band radiometer observations were presented in this paper in order to demonstrate the effectiveness of time and frequency domain blanking for RFI mitigation. The L-band Canton campaign included observations in the presence of a pulsed radar system, and show the effectiveness of the real-time APB approach for mitigating pulsed sources. C-band data from an airborne campaign demonstrated that even low-level RFI could be successfully mitigated with a fairly simple cross-frequency blanking algorithm. In both

cases, examples were shown in which the use of high time and/or frequency resolution allowed the detection and mitigation of RFI whose signature on larger time or frequency scales was comparable to the instrument sensitivity and expected geophysical variations.

Future campaigns are planned to provide observations over more diverse environments and to allow intercomparison with other RFI mitigation techniques (as already reported in [9] for a comparison of cross-frequency blanking at low and high frequency resolution.) Simulations of expected RFI contributions due to particular sources (as in [14]-[15], for example) can be utilized as well to allow prediction of the expected performance of time and frequency blanking methods. It is hoped these studies will find application in future air and space borne systems for passive microwave sensing of the Earth.

ACKNOWLEDGMENT

The support of personnel from the University of Michigan (led by Prof. Chris Ruf) in the Canton campaign is acknowledged, as well as the support of the PSR/CXI team from the University of Colorado (led by Prof. Al Gasiewski). This work was performed under the sponsorship of a NASA Instrument Incubator Program project (led by the University of Michigan) and the National Polar-Orbiting Operational Environmental Satellite System (NPOESS) Integrated Program Office.

REFERENCES

[1] L. Li, E. G. Njoku, E. Im, P. S. Chang, and K. M. St.Germain, "A preliminary survey of radio-frequency interference over the US in Aqua AMSR-E data," *IEEE Trans. Geosc. Rem. Sens.,* vol. 42, pp. 380-390, 2004.

[2] S. W. Ellingson and J. T. Johnson, "A polarimetric survey of radio frequency interference in C- and X-bands in the continental United States using WindSAT radiometry," *IEEE Trans. Geosc. Rem. Sens.,* vol. 44, pp. 540–548, 2006.

[3] A. J. Gasiewski, M. Klein, A. Yevgrafov, and V. Leuski, "Interference mitigation in passive microwave radiometry," *IEEE Geoscience and Remote Sensing Symposium,* conference proceedings, vol. 3, pp. 1682-1684, 2002.

[4] M. Basseville and I. V. Nikiforov, *Detection of abrupt changes: theory and applications.* Englewood Cliffs, NJ: Prentice-Hall, 1993.

[5] P. A. Fridman and W. A. Baan, "RFI mitigation methods in radio astronomy," *Astronomy&Astrophysics,* vol. 378, pp. 327-344, 2001.

[6] C. S. Ruf, S. M. Gross, and S. Misra, "RFI detection and mitigation for microwave radiometry with an agile digital detector," *IEEE Trans. Geosc. Rem. Sens.,* vol. 44, pp. 694-706, 2006.

[7] G. A. Hampson, S. W. Ellingson, and J. T. Johnson, "Design and demonstration of an interference suppressing microwave radiometer," *IEEE Aerospace Conference,* conference proceedings, vol.2, pp. 993-999, 2004.

[8] J. T. Johnson, B. Güner, and N. Niamsuwan, "Observations of an ARSR system in Canton, MI with the L-band interference suppressing radiometer,"project report, Dec 2005. (available at `http://esl.eng.ohio-state.edu/~rstheory/iip/lisr_jtj.pdf`)

[9] J. T. Johnson, A. J. Gasiewski, B. Güner, G. A. Hampson, S. W. Ellingson, R. Krishnamachari, N. Niamsuwan, E. McIntyre, M. Klein, and V. Y. Leuski, "Airborne radio-frequency interference studies at C-band using a digital receiver," *IEEE Trans. Geosc. Rem. Sens.*, vol. 44, pp. 1974-1985, 2006.

[10] J. T. Johnson, A. J. Gasiewski, B. Güner, M. Valerio, and M. Klein, "High altitude measurements of C-band radio frequency interference using a digital Receiver," *IEEE Geoscience and Remote Sensing Symposium,* conference proceedings, pp. 2301-2304, 2006.

[11] J. T. Johnson, B. Güner, N. Niamsuwan, and M. Valerio, "Airborne C-band RFI measurements with PSR/CXI and CISR from the WB-57 aircraft: initial data examination,"project report, March 2006. (available at `http://www.ece.osu.edu/~johnson/cisr/cisr060123.pdf`)

[12] N. Niamsuwan, B. Güner, and J. T. Johnson, "Observations of an ARSR system in Canton, MI with the L-band interference suppressing radiometer," *IEEE Geoscience and Remote Sensing Symposium,* conference proceedings, pp. 2285-2288, 2006.

[13] N. Niamsuwan, J. T. Johnson, and S. W. Ellingson, "Examination of a simple pulse blanking technique for RFI mitigation" *Radio Science,* vol. 40, June 2005.

[14] LeVine, D. M., "ESTAR experience with RFI at L-band and implications for future passive microwave remote sensing from space," *IEEE Geoscience and Remote Sensing Symposium,* conference proceedings, pp. 847–849, 2002.

[15] Camps, A., I. Corbella, F. Torres, J. Bara, and J. Capdevila, "RF interference analysis in aperture synthesis interferometric radiometers: application to L-band MIRAS instrument," *IEEE Trans. Geosc. Rem. Sens.,* vol. 38, pp. 942–950, 2000.